Nano Research

Open Access

Research Article

Custom-assembled phase change modular devices for personalize speciality: Carbon energy thermal management application

Yilin Chen[1], Huitao Yu[1], Yiyu Feng[1,2] ✉, and Wei Feng[1,2] ✉

[1] *School of Materials Science and Engineering and Tianjin Key Laboratory of Composite and Functional Materials, Tianjin University, Tianjin 300350, China*
[2] *Institute of Advanced Technology and Equipment, Beijing University of Chemical Technology, Beijing 100029, China*

Cite this article: *Nano Research*, **2025**, *18*, 94907202. https://doi.org/10.26599/NR.2025.94907202

ABSTRACT: In the context of 5G, the high-frequency cyclicity and inhomogeneity of heat flow put forward higher requirements for the thermal control system of electronic devices, and there is a great need for thermal management modules with fixed point and high efficiency to ensure the long-term development of electronic devices. Here, we selected four phase change molecules with significant differences in phase change temperatures to be composited with graphene aerogel (GA) to obtain Ei@GA, Tetra@GA, Octa@GA, and 1,10-Deca@GA. Compared with pure phase change molecules, the thermal conductivity has been increased by more than 20%, and the relative enthalpic efficiency is as high as 98.7% or more. Further, we assembled the four phase change composites by "reduction welding" to obtain the integrated, modular thermal management device M_1-PCMs@GA. Simulation of inhomogeneous heat generation in electronics by building an inhomogeneous heat generation platform. Compared with the homogeneous modules M_2-Ei@GA and M_3-1,10-Deca@GA, the effective temperature control time of the customized module M_1-PCMs@GA is extended by 100.0 and 394.3 s, respectively. Therefore, custom-assembled modular thermal management devices have important application prospects in the field of intelligent temperature control of electronic devices, and the idea of cascade assembly enriches the application functions and development direction of intelligent thermal managers.

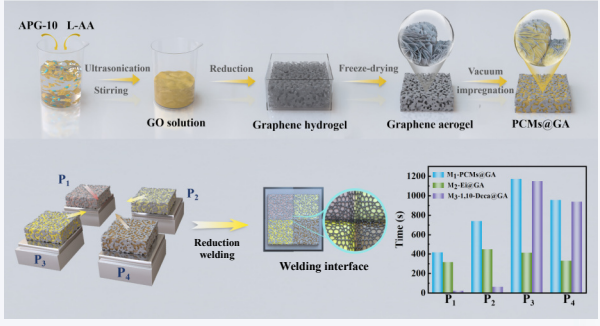

KEYWORDS: graphene aerogel, phase change materials, assembly customization, modular thermal management devices

1 Introduction

Driven by the functionalization, miniaturization, and ultra-high integration of electronic devices [1–6], the ultra-high heat flux density (100 W/cm^2) that electronic devices should have causes their temperatures to rise dramatically in a relatively short period of time. It also undergoes high-frequency thermal cycling, which shortens the life of the electronics, corrupts the data or even fails [7–9]. Referring to the Arrhenius equation, it can be seen that for every 10 °C rise in the chip, the operating life is halved. High temperatures also lead to a decrease in the mechanical properties of metallic materials and a risk of breakdown of semiconductor materials [10, 11]. Therefore, it is urgent to develop effective temperature control techniques for electronic components. Phase change material is a material that is capable of storing or releasing large amounts of latent heat during the occurrence of a simple physical phase transition, while undergoing only minor volume changes and maintaining a constant temperature [12–14]. This material exhibits advantages such as high enthalpy of phase change, excellent chemical stability, non-toxicity, and non-corrosiveness [15–18], leading to its widespread application in areas including industrial waste heat recovery, aerospace, building insulation, solar energy utilization, and personal thermal management [19–25]. Notably, in the realm of thermal management for electronic devices, the phase change material (PCM) thermal management process operates passively without requiring external power, thereby enhancing the safety and stability of systems [26]. Additionally, PCMs possess high energy density, facilitating the miniaturization and weight reduction of electronic devices, thus meeting the dual demands of portability and high performance in contemporary electronics. Nevertheless, challenges persist regarding

Received: November 27, 2024; **Revised:** December 17, 2024
Accepted: December 18, 2024

✉Address correspondence to Yiyu Feng, fengyiyu@tju.edu.cn; Wei Feng, weifeng@tju.edu.cn

the low thermal conductivity and potential leakage of PCMs [27, 28], as well as issues of poor long-term stability, supercooling, and phase separation that remain unresolved [26]. Many studies have been reported on the improvement of thermal conductivity of phase change materials using the approach of compositing with porous thermally conductive materials, such as graphene aerogel, porous polymer-based materials, carbon nanotube sponges, porous carbon, boron nitride, and foamed metals [29–35]. Cao et al. [36] prepared a phase change composite utilizing the MXene/polyimide (MXene/PI) aerogel poly(ethylene glycol) (PEG) phase change composite MXene/PI@PEG with good shape stability, and also exhibited excellent photothermal conversion ability due to the incorporation of MXene, with an enthalpy as high as 167.9 J/g and a relative enthalpy efficiency of 99.8%. Wu et al. [37] developed a strategy to synthesize highly thermally conductive phase change composites by inducing a large aligned graphite flake structure by compression within phase change composites (PCCs). An increase in thermal conductivity in the range of 4.4–35.0 W/(m·K) was achieved with less than 40.0 wt.% graphite loading. Graphene possesses exceptional mechanical and electrical properties, outstanding thermal conductivity, and favorable processability, making it a promising material for applications in the field of electronic devices [38–40]. Yu et al. [41] used laser-induced polymer carbonization to directly make graphene, greatly reducing the manufacturing cost of graphene and expanding the application of graphene in flexible electronic devices. And graphene aerogel is frequently selected as a matrix for phase change composites due to its lightweight nature, high thermal conductivity, high elasticity, thermal stability, and large specific surface area [42, 43], which can simultaneously improve its thermal conductivity and prevent leakage.

Also more noteworthy is the fact that in the particular context of the use of electronic devices, higher power densities tend to occur locally, leading to localized temperatures above normal operating thresholds and large temperature gradients within the electronic device through heat transfer from the substrate [44, 45]. Against the backdrop of rapidly evolving performance in all aspects of electronics, electronic device thermal management materials must be able to cope with heat dissipation at various operating temperatures, maintain relatively stable temperatures under high-frequency heat cycling, and manage device heat generation imbalances in a gradient manner. Single-temperature thermal management materials are no longer adapted to the heat generation characteristics of most electronic devices [46, 47]. However, there are fewer studies on how to solve localized high power heating and overall gradient temperature control using phase change composites. Therefore, there is an urgent need for thermal management devices with fixed-point and modular temperature thermal management functions for directional thermal management and delaying the thermal response of the device.

Yang et al. [48] investigated the heat transfer characteristics of phase change molecules arranged in cascade, and showed that cascading the phase change molecules according to their thermal conductivity could enhance the heat dissipation by 220.8%. This made us realize that traditional homogeneous phase change composites are no longer suitable for today's increasingly complex thermal scenarios, and inspired us to tailor the assembly of thermal management materials to the thermal characteristics of electronic devices. In this paper, a novel modular phase change composite material is prepared, which can control the uneven heat generation of electronic devices in a fixed point and quantitative manner, so as to maximize the thermal management efficiency. Graphene aerogels (GAs) with three-dimensional continuous through holes with a pore size of about 100 mm and a porosity of 95.09% were firstly prepared using the foaming method [49, 50] and freeze-drying. The capillary action [51] was utilized to effectively prevent the phase change molecules from leaking, and the three-dimensional skeleton provided a continuous thermal conductivity pathway.

The thermal conductivities of the prepared graphene aerogel phase change composites (PCMs@GA) were increased by 20%–27% compared with the pure phase change materials, and the latent heat of phase change was 209.5, 232.4, 245.5, and 263.1 J/g, with the relative enthalpy efficiencies exceeding 98.7%. After 50 cycles, the enthalpy of phase change is reduced by less than 1%. In addition, the thermal management module M_1-PCMs@GA was prepared by "reduction welding" based on the arrangement and assembly of different kinds of phase change molecules, which has better temperature control effect than the homogeneous phase change composite modules M_2-Ei@GA and M_3-1,10-Deca@GA, and the effective temperature control time was extended by 100.0 and 394.7 s, respectively. The modularized temperature control device proposed in this study has important application prospects in the field of intelligent temperature control and prevention of thermal damage in electronic devices, and the concept enriches the application functions and development direction of intelligent thermal managers.

2 Experiment

2.1 Materials

Graphene oxide (GO) was prepared using a modified Hummers method [52]. Among them, 325 mesh natural graphite was purchased from Tianjin Damao Chemical Reagent Co. in China. Sodium nitrate ($NaNO_3$), potassium permanganate ($KMnO_4$), concentrated sulfuric acid (H_2SO_4), hydrogen peroxide (H_2O_2), concentrated hydrochloric acid (HCl) were purchased from Tianjin Jiangtian Chemical Technology Co. L-Ascorbic acid (L-AA) was purchased from Shanghai Myriad Chemical Technology Co. Alkylglycosides (APG-10) were provided by Shanghai Aladdin Reagent Co. n-Eicosane, n-tetracosane, n-octacosane and 1,10-decanediol were purchased from TCI (Shanghai) Chemical Industry Development Co., Ltd. with a purity of > 98%. Hydrazine hydrate was purchased from Tianjin Hiens Biochemical Technology Co. Ltd. with a purity of 80%. Deionized water was prepared in the laboratory.

2.2 Materials characterization

The morphology and microstructure of graphene aerogels and composites were observed by scanning electron microscopy (SEM, JSM-7800F, JEOL). The crystallization behavior of the samples was investigated by X-ray diffraction (XRD, Empyrean-100, Panalytical). Raman spectra were obtained using a Raman microscope system (Horiba LabRAM HR Evolution) with 633 nm laser excitation. An X-ray photoelectron spectrometer (Thermo Fisher Scientific Nexsa G2) was used to test the C and O elemental ratios of GO and GA. The porosity and pore size distribution of GA were determined using a high-performance fully automated mercury piezometer (AutoPore Iv 9510). Fourier transform

infrared spectroscopy (FTIR, iS50, Nicolet) was used to detect the chemical structure evolution and compatibility of the samples in the wave number range of 4000–400 cm^{-1}. The relevant phase transition parameters and specific heat capacities were measured by differential scanning calorimeter (Discovery DSC, TA, America) under nitrogen atmosphere with heating and cooling rates of 10 °C/min. Solid-state thermal conductivity was tested by laser thermal conductivity meter (LFA-467, NETZSCH) at room temperature of 25 °C. The thermal conductivity of the samples was measured by laser thermal conductivity meter (LFA-467, NETZSCH). Thermogravimetric analyzers (TGA, SETSYS 16/18, SETARAM) were used to test the thermal stability of phase change composites. A Keithley digital multi-meter (Keithley 2001) connected to a SIN-R9600 thermocouple (SIN-R9600, Sinomeasure) was used for real-time temperature monitoring to record the phase change heat transfer process.

2.3 Preparation of graphene aerogel thermally conductive matrix (GA)

First, 40 mL of homogeneously dispersed GO solution (7 mg/mL) was obtained by ultrasonication in a 100 mL beaker, and 480 mg of L-ascorbic acid was added as a reducing agent. Then 0.21 g of alkylglycoside (APG-10) 50% aqueous solution was added for foaming with vigorous stirring at high speed (2000 rpm) for 5 min, and the foaming rate was about 1.5 times. After that, the foamed GO solution was poured into a sealed mold and heated in an oven at 80 °C for 12 h to obtain a graphene hydrogel. It was washed with deionized water for three times and then placed in the refrigerator for complete freezing, and then freeze-dried in a lyophilizer for 24 h to obtain GA. Annealing at 500 °C for 1 h was also performed to improve its thermal conductivity.

2.4 Preparation of phase change composite (PCMs@GA)

PCMs@GA were prepared by infiltrating phase change materials into graphene aerogels using a vacuum-assisted impregnation method. Specifically, the phase change material was heated to 20 °C above its melting point until all of it was molten, and the GA was placed in the molten phase change material and impregnated under vacuum for 24 h, with repeated vacuuming during the process until it was fully permeated. The excess phase change molecules were removed and wiped off the surface to obtain PCMs@GA by natural cooling. For most electrical components, the normal operating temperature range is usually between −40–85 °C [53]. The types of phase change materials selected for this temperature range and for the properties of the phase change molecules themselves are n-eicosane, n-tetracosane, n-octacosane and 1,10-decanediol.

2.5 Preparation of modular phase change composites (M-PCMs@GA)

The steps for preparing customizable assembled modular phase change composites by reduction welding are as follows: a GO solution with a concentration of 10 mg/mL is prepared, applied to the side of the blocks to be spliced, and 0.2 mL of hydrazine hydrate solution is added dropwise to ensure that the spliced blocks are in close contact, and a certain amount of pressure is given and placed in the oven at 40 °C for 20 min to complete the welding [54]. It is worth noting that, since the organic phase change molecules and graphene oxide do not infiltrate each other, in order to achieve the purpose of splicing assembly, we heat the interface to be spliced in advance, so that a small portion of the phase change molecules leaks out, revealing the graphene aerogel that is covered by them. At this point, the graphene aerogel can be well infiltrated with the graphene oxide solution, and the splicing assembly can be realized in the subsequent reduction welding. In this method, the raw material is consistent with the matrix, and a thin graphene layer is formed without destroying the structure of the phase change composite. The raw material of the method is consistent with the matrix, and a thin graphene layer is formed without destroying the phase change composite structure. This customizable, integrated composite device holds great promise for practical thermal management applications.

3 Results and discussion

3.1 Morphological structure of GA and phase change composites

Figure 1 illustrates the preparation procedure for PCMs@GA composites. GO nanosheets were uniformly dispersed via ultrasonication in deionized water to produce a viscous GO solution. Subsequently, foaming was initiated by vigorous stirring upon the addition of reducing and foaming agents, resulting in the formation of numerous microbubbles within the solution. Due to surface tension, the GO nanosheets were dispersed around these microbubbles. The mixture was then poured into a sealed container and subjected to heating, during which the GO nanosheets underwent reduction and interconnected to form a hydrogel under the influence of the reducing agent. The resultant hydrogel was subsequently freeze-dried to yield a graphene aerogel characterized by a three-dimensional network of interconnected pores. In a vacuum oven, PCMs infiltrate the graphene aerogel through capillary action, achieving a high filling rate.

In the study of improving the thermal conductivity of phase change molecules using thermally conductive substrates, a continuous three-dimensional skeleton plays a decisive role in the construction of a good thermal conductivity pathway. Therefore, in order to study the microscopic pore structure inside the prepared GA, we performed SEM tests. Figure 2(a) shows the optical picture of the prepared graphene aerogel, which shows that the aerogel by freeze-drying is well molded and has a very low mass. Figures 2(b) and 2(c) show the cross-section SEM images of the GA, which can clearly observe the structure and distribution of the internal pores, and it can be seen that the pore size distribution of the aerogel prepared by high-speed stirring and foaming is relatively uniform and presents interconnected macropore, and this three-dimensional interconnection network assembled by p–p interactions is conducive to the phonon conduction [55] (Fig. 2(d)). The porosity of the aerogel was 95.09% as measured by piezomercury method, and the pore diameter was about 100 μm, and the large porosity provided sufficient space for filling phase change molecules. Figure 2(e) shows the cross-section scan of the phase change composite after vacuum impregnation, and it can be seen that the phase change molecules are completely encapsulated in the aerogel skeleton with a high filling rate, which is attributed to the large surface tension and capillary action of GA. Figure 2(f) shows the Fourier infrared spectra before and after impregnation. The broad peaks observed in the range of 3647–3331 cm^{-1} for graphene aerogel after reduction correspond to the stretching vibrations of –OH groups. The vibrational absorption peaks associated with C–O–C are found between 1099–1017 cm^{-1}, while the stretching vibrational peaks of the C=O double bond from carboxyl groups

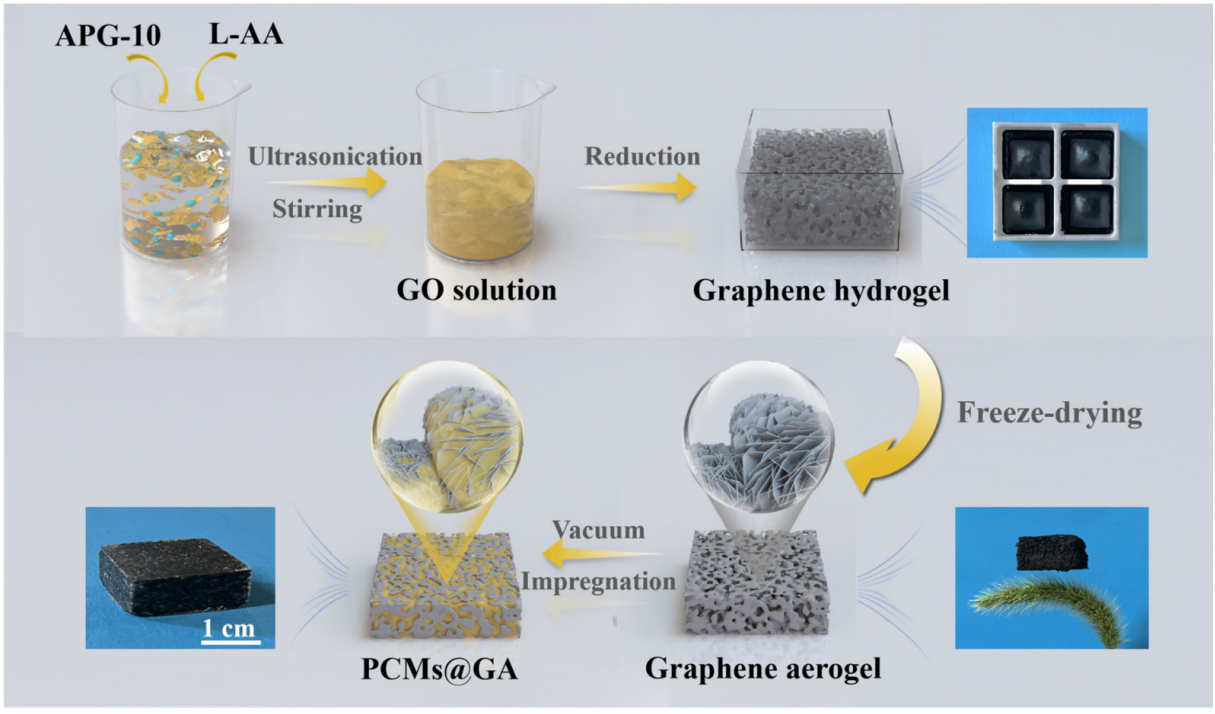

Figure 1 Schematic representation of the manufacturing process of PCMs@GA composites.

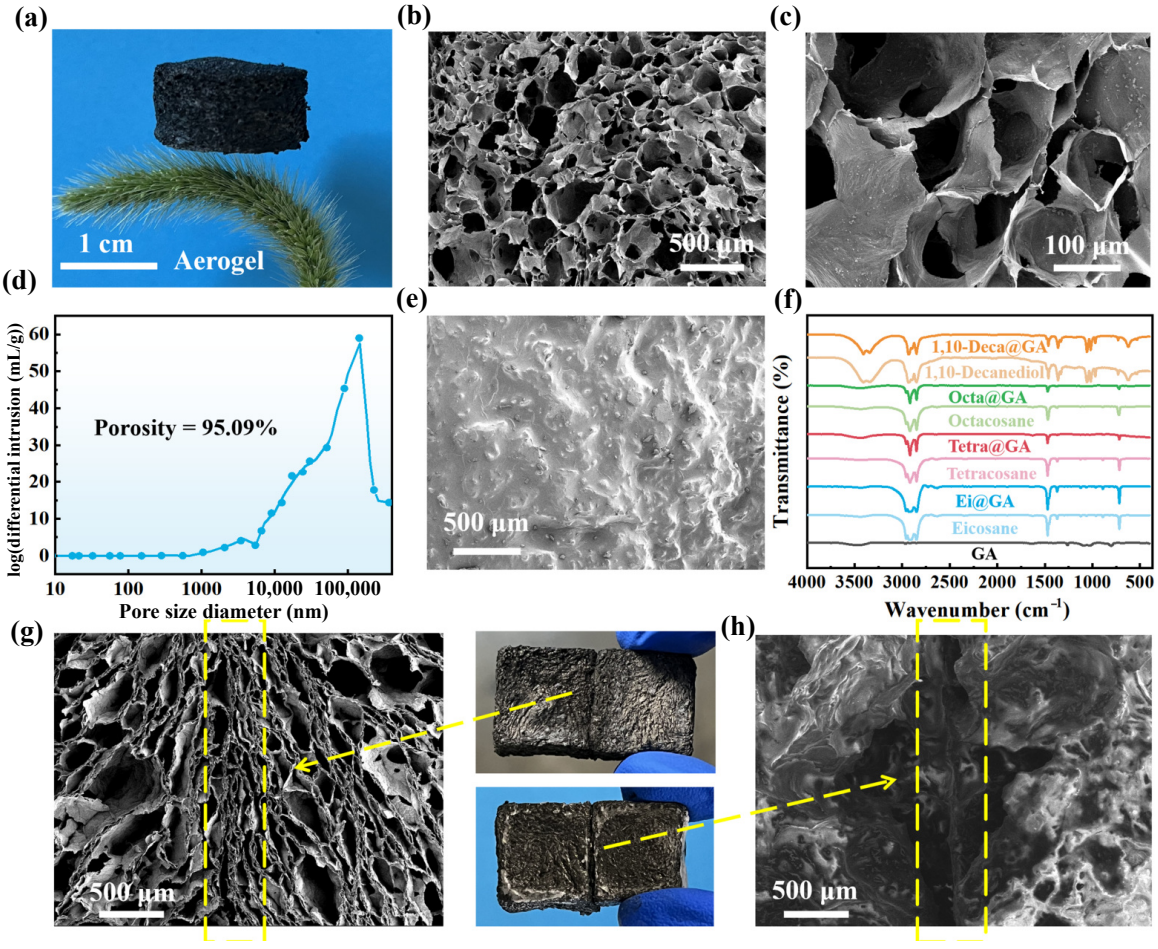

Figure 2 (a) Photograph of graphene aerogel. (b) and (c) Scanning electron microscope images of the internal pores of graphene aerogel. (d) Measurement of pore size and porosity of graphene aerogel by high-performance fully automated mercuric pressure meter. (e) Scanning electron micrograph of the cross-section of the impregnated phase change composite. (f) Fourier infrared spectra of phase change molecules and corresponding composites. (g) Optical photographs and scanning electron microscopy of graphene aerogel reduction welds. (h) Optical photograph and SEM image of the impregnated phase change composite at the reduction weld.

present in GO nearly vanish around 1675 cm^{-1}. This indicates that the graphene aerogel we prepared exhibits a high degree of reduction; however, some oxygen-containing functional groups remain. n-Eicosane, n-tetracosane, and n-octacosane all display –CH stretching vibration peaks within the range of 2960–2846 cm^{-1}, as well as –CH bending vibration peaks at approximately 1470 and 1372 cm^{-1}. The absorption peaks for 1,10-decanediol appear at 3407–3336 cm^{-1}, corresponding to –OH stretching vibrations. Additionally, there are absorption peaks ranging from 1056–970 cm^{-1} attributed to C–O stretching vibrations and a bending vibration for –OH near 623 cm^{-1}. In conclusion, the composite material showed only minor changes at the –OH absorption peaks from 3647 to 3331 cm^{-1}。

Vacuum impregnation is a complete physical composite and does not affect the structural and thermal properties of the phase change molecules. Figures 2(g) and 2(h) show optical pictures and SEM images of the aerogel interface spliced using reduction welding and the composite spliced interface after impregnation, presenting a thin graphene film at the spliced area with a denser weld. The advantage of this joining method is that the raw material is consistent with the matrix and does not affect the phase transition properties. This GA with high porosity and interconnected macropores has excellent performance in encapsulating phase change molecules and improving thermal conductivity. Figure S1 in the Electronic Supplementary Material (ESM) shows the structural characterization of graphene sheets and graphene aerogels.

3.2 Thermal conductivity and phase transition process of PCMs@GA

Organic phase change materials have messy heat conduction paths and low thermal conductivity due to their complex internal crystallization directions. It is an important challenge that limits its application. We tried to improve its thermal conductivity by introducing graphene aerogel skeleton. Figure 3(a) demonstrates the schematic diagram of the fabrication process of PCMs@GA composites. In addition, we have investigated the thermal conductivity of phase change composites using laser thermal conductivity meter as shown in Fig. 3(c). The thermal conductivity of the pure phase change molecules is low, while most of the defects inside the graphene aerogel, which has been reduced and annealed at high temperatures in the composite, are repaired, which is favorable for phonon conduction. The thermal conductivities of the four composites were enhanced to 0.227, 0.252, 0.238, and 0.368 W/(m·K), respectively, with the enhancement rates of 26.30%, 26.10%, 25.05%, and 20.85%.

The law of latent heat absorption at different temperatures for phase change materials is determined by the nature of the material. Phase change materials should be selected according to different properties and application scenarios to prepare subsequent modular thermal management devices. In order to investigate the actual temperature control ability of the four PCMs@GA prepared as described above, the four phase change composites were placed on a hot bench at 110 °C to record the top surface temperature versus time curves. Figure 3(b) displays the pictures of the changes of the four phase change composites taken with an infrared thermal imager. Ei@GA, Tetra@GA, Octa@GA, and 1,10-Deca@GA increase in heat-absorbing capacity in that order, which corresponds to a sequential prolongation of the time when the phase transition occurs. Figure 3(d) shows the temperature versus time curves of the four composites. For the first 50 s, the temperature of Ei@GA remains almost constant due to the phase transition, while the temperatures of Tetra@GA, Octa@GA, and

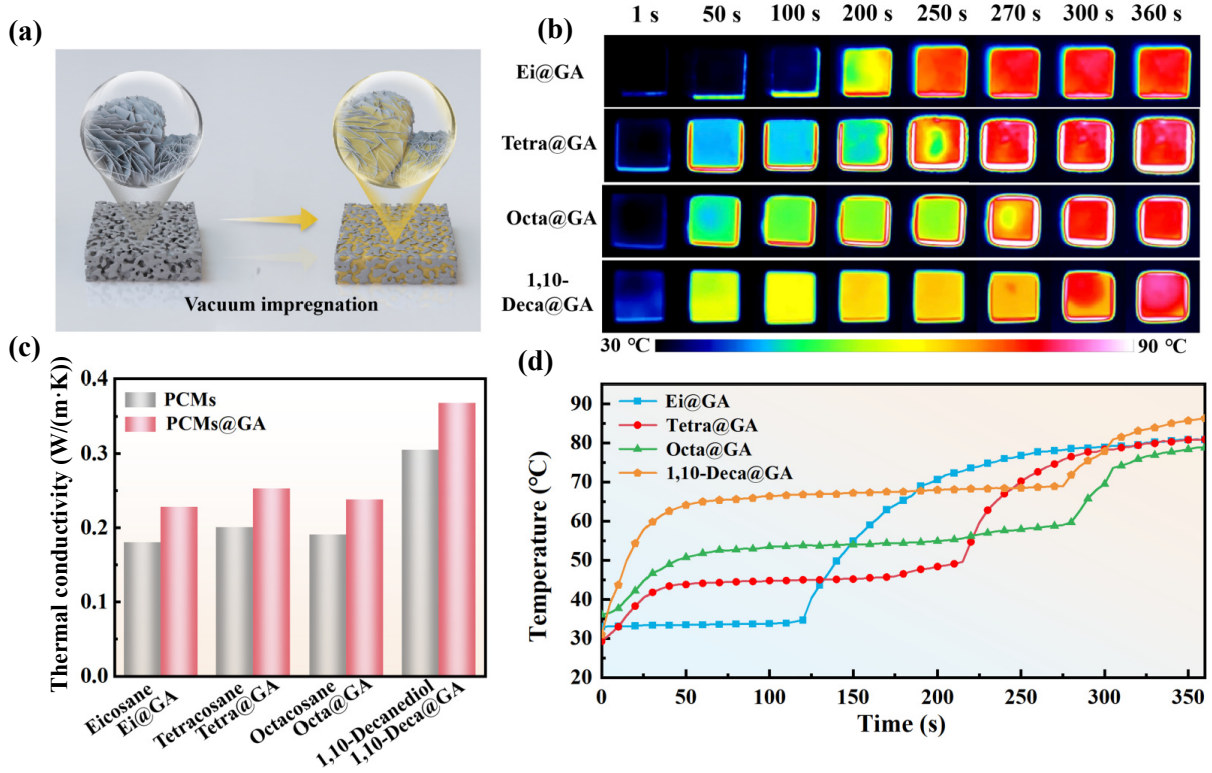

Figure 3 (a) Schematic diagram of the fabrication process of PCMs@GA composites. (b) Infrared thermography picture of PCMs@GA over time. (c) Thermal conductivity of phase change molecules and corresponding composites. (d) Curve of the top surface temperature of PCMs@GA on the hot bench at 110 °C with time.

1,10-Deca@GA increase rapidly because they have not yet reached their phase transition temperatures, and the temperature of Ei@GA is the lowest at this time. And because the phase transition enthalpy of Ei@GA is the lowest, around 120 s, Ei@GA completes the whole phase transition process, and the length of the plateau period is about 120 s. After that, the temperature rises rapidly, and the temperature becomes the highest among the four phase-transition composites at about 190 s. Therefore, Ei@GA is suitable for low-temperature and short-time thermal control. The phase transition process of Tetra@GA basically ends at about 215 s. The plateau period is about 185 s, and it enters into the stage of rapid warming. Octa@GA and 1,10-Deca@GA complete the phase transition process at 270 and 280 s, respectively, and the plateau period is about 240 and 250 s. The temperature of 1,10-Deca@GA exceeds the temperature of the remaining three composites around 300 s. And the temperatures of all four phase change composites exceeded 80 °C at 360 s. In conclusion, considering the interfacial thermal resistance and heat dissipation, the phase change composites are suitable to be applied in environments that are 15–20 °C above their phase change temperatures, and can control the temperature around their own phase change temperatures for a longer period of time. That is, Ei@GA is suitable for temperature control around 52 °C, Tetra@GA is suitable for temperature control around 67 °C, Octa@GA is suitable for temperature control around 79 °C, and 1,10-Deca@GA is suitable for temperature control around 92 °C. The four phase change molecules with different phase change laws provide the basis for subsequent customization of modular phase change composite devices.

3.3 Thermophysical properties, cycling stability and thermal stability of PCMs@GA

In thermal management applications, the enthalpy of phase change of a phase change material is a key indicator of its ability to absorb/export heat. A high enthalpy of phase change is the basis for keeping the temperature relatively constant for a long time. The melting/crystallization processes of n-eicosane, n-tetracosane, n-octacosane and 1,10-decanediol and their composites (PCMs@GA) were investigated by DSC as shown in Figs. 4(a) and 4(b). In DSC curve (Fig. 4(a)), all four phase change molecules show a sharp single peak of melting, while the melting peak broadens and shifts to the right after compositing with graphene aerogel, which is attributed to the homogeneous heat dispersion by the GA skeleton and slows down the melting process. During the crystallization process in Fig. 4(b), n-eicosane, n-tetracosane, n-octacosan showed double crystallization peaks, indicating that they have two different crystallization modes. 1,10-decanediol crystallization peaks were

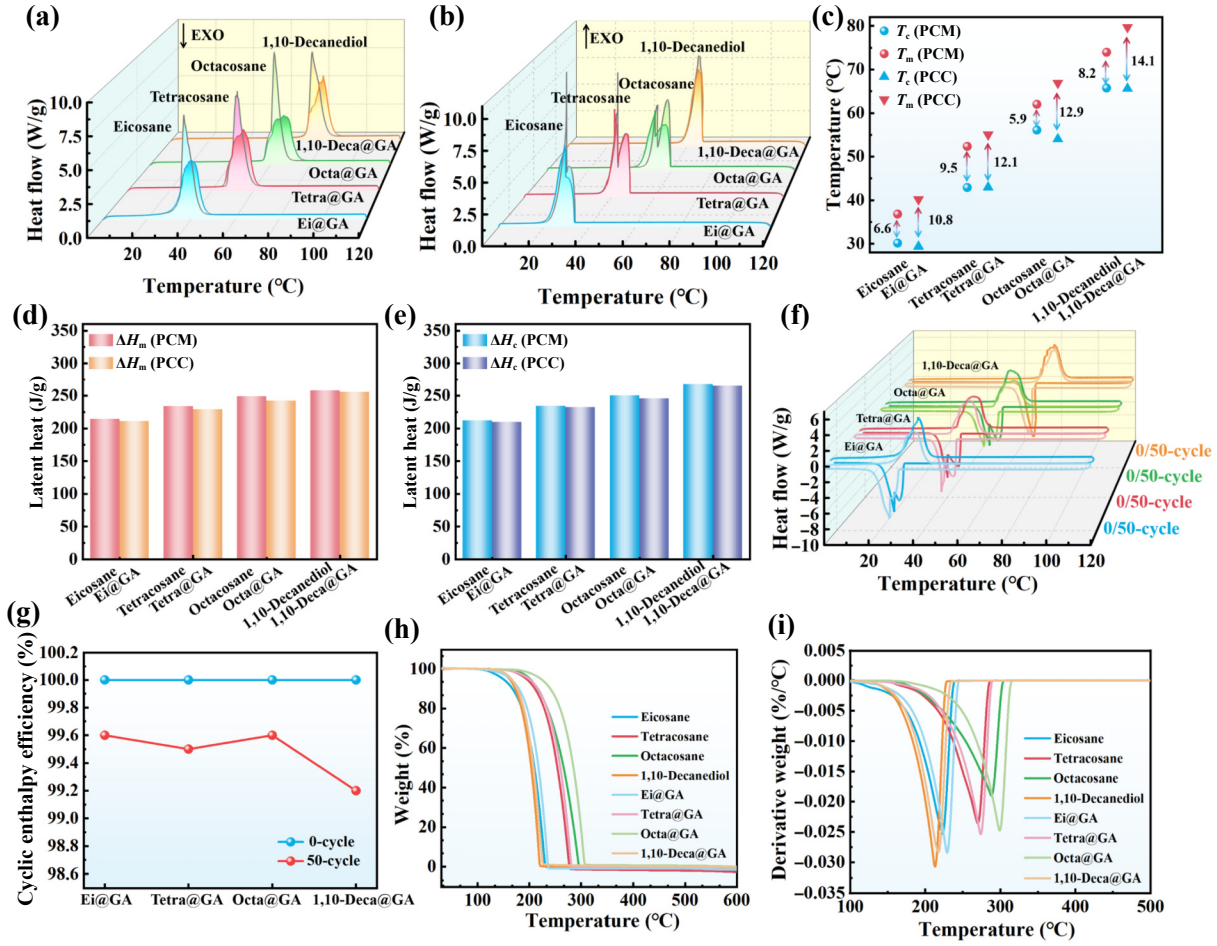

Figure 4 (a) DSC melting peak curves of phase change molecules and corresponding composites. (b) DSC crystallization peak curves of phase-change molecules and corresponding composites. (c) Melt enthalpy comparison of phase change molecules and corresponding composites. (d) Comparison of the enthalpies of crystallization of phase-change molecules and corresponding composites. (e) Comparison of melting temperature, crystallization temperature and supercooling degree of phase change molecules and corresponding composites. (f) DSC curves of phase change composites after 50 cycles. (g) Cyclic enthalpy efficiency curves of phase change composites after 50 cycles. (h) TG curves of phase change molecules and corresponding composites. (i) DTG curves for phase change molecules and corresponding composites.

single peaks. However, the same as the melting peak, the crystallization peak becomes tonal after complexing with GA, with a tendency of left shift. Figure 4(c) shows the variation of phase transition temperature of the phase transition molecules and their composites. The phase transition temperatures of n-eicosane, n-tetracosane, n-octacosane and 1,10-decanediol increased sequentially, which were 36.8, 52.4, 62.0, and 74.0 °C, respectively. The differences are obvious and can be chosen for different scenarios. Figures 4(d) and 4(e) show the histograms of melting enthalpy and crystallization enthalpy of phase change molecules and their composites, respectively. The enthalpies of melting/crystallization (ΔH_m/ΔH_c) are all higher, i.e., higher heat absorption/expulsion capacity, which enables temperature control for a long time in subsequent applications. Table S1 in the ESM lists the specific thermophysical property data for PCMs and PCMs@GA. The enthalpies of the composite phase change materials decreased after the introduction of graphene aerogel backbone, which was attributed to the fact that the aerogel backbone (GA) does not have latent heat and would hinder the melt crystallization process of the phase change molecules to some extent. For this reason, we introduce the concept of relative enthalpy efficiency (η) to evaluate the phase change performance of composite materials as in Eq. (1)

$$\eta = \frac{\Delta H_m(\mathrm{PCC}) + \Delta H_c(\mathrm{PCC})}{(\Delta H_m(\mathrm{PCM}) + \Delta H_c(\mathrm{PCM})) \times \omega\mathrm{PCM}} \times 100\% \quad (1)$$

where ΔH_m(PCC) and ΔH_c(PCC) represent the enthalpy of melting and crystallization of the composite, and ΔH_m(PCM) and ΔH_c(PCM) represent the enthalpy of melting and crystallization of the phase change material. ωPCM denotes the weight percentage of phase change molecules in the PCC. Due to the light weight of GA skeleton and its relatively small proportion in composite materials, it is calculated that the relative enthalpy efficiencies of PCMs@GA are all above 98.7%, and the specific data are shown in Table S1 in the ESM.

Cycle stability is an important parameter of phase change composites, and good cycle stability is very necessary for long-term use of PCC. Figure 4(f) demonstrates the DSC curves of four PCM composites after 0 cycles and 50 cycles. Slight differences in the DSC curves were observed during the melting/crystallization behavior of 50 cycles. As shown in Fig. 4(g), the cyclic enthalpy efficiency of Ei@GA, Tetra@GA and Octa@GA only decreased by less than 0.5% after 50 cycles. The cyclic stability of 1,10-Deca@GA is slightly worse than that of the first three kinds, and the cyclic enthalpy efficiency decreases by 0.8% after 50 cycles. In addition, thermogravimetric analysis (TG) tests were performed to test the thermal stability of the composites. In Fig. 4(h) TG curves, it can be seen that n-Eicosane has the worst thermal stability and is the first to undergo thermal decomposition at around 110 °C, followed by 1,10-decanediol. n-tetracosane, n-octacosane are more thermally stable and decompose at about 150 and 157 °C, respectively, with final decomposition temperatures of 239 and 247 °C. The initial decomposition temperatures and final decomposition temperatures of Ei@GA, Tetra@GA, Octa@GA, and 1,10-Deca@GA were right-shifted after the introduction of graphene aerogel skeleton. Similarly, in the DTG plots of Fig. 4(i), the decomposition temperatures were also right-shifted, which was attributed to the fact that the 3D graphene aerogel skeleton could transfer the heat well and uniformly, resulting in the improvement of the composites' thermal stability. The above results consistently confirm that the prepared PCMs@GA have better heat storage capacity, cycling stability and thermal stability, and have a bright application prospect in the field of thermal management.

3.4 Thermal management performance of M-PCMs@GA in uneven heat generation scenarios

Existing phase change thermal management elements have a single temperature control range, while the heat generation of electronic devices is uneven, in order to solve this contradiction, we propose to use customized spliced modular phase change composites for directional thermal management, which is beneficial to delay the thermal response of the device and break through the constraints of heat dissipation problems on the development of the performance of electronic devices. We built a four-quadrant test bench with different temperatures to simulate multi-point heat generation at different power levels. From left to right, from top to bottom, the four regions P_1, P_2, P_3 and P_4, were set to 52, 67, 79, and 92 °C, respectively, corresponding to 15–20 °C above the melting temperature of the four phase change molecules. Combined with the reality, the use temperature of the transistor should be no higher than 70 °C [56], so we set the ideal temperature control temperature of the four regions to be no more than 35, 50, 60, and 70 °C on the top surface, respectively.

As shown in Fig. 5(a), a modular thermal management device M_1-PCMs@GA is fabricated by reduction welding method, which is composed of Ei@GA, Tetra@GA, Octa@GA and 1,10-Deca@GA. Two uniform comparison modules are prepared by the same method, namely M_2-Ei@GA formed by four pieces Ei@GA, and M_3-1,10-Deca@GA formed by four pieces 1,10-Deca@GA. Table S2 in the ESM shows the specific dimensions and quality information for the three modules. The structures are schematically shown in Fig. 5(b). We recorded the top surface temperature change curves with time for the three thermal management modules as shown in Figs. 5(c)–5(e). In Fig. 5(c), due to the selection of suitable phase change materials for the four regions of heat generation power, the curves can display a clear gradient and a phase change plateau in the corresponding phase change temperature interval, which can keep the temperature relatively stable for a longer period of time (292, 597, 942, and 855 s) during the plateau period. In Fig. 5(d), M_2-Ei@GA is a composite consisting of four identical Ei@GA, all of which show a plateau near 35 °C. However, due to the low enthalpy of phase transition of n-eicosane, the plateau period decreases sequentially with the temperature increase, which makes it difficult to achieve a long time of temperature control, and the high-temperature region breaks through the upper limit of the set temperature rapidly after the complete phase transition. In Fig. 5(e), M_3-1,10-Deca@GA is a composite consisting of four identical pieces of 1,10-Deca@GA. During the initial 100 s, the temperatures of all four quadrants increase sharply, and it is noteworthy that the P_2 region temperature T_2" of M_3-1,10-Deca@GA exceeds the P_3 region temperature T_3". This is due to the fact that in the initial period, the temperatures of regions P_1, P_2, and P_3 have not reached the phase transition temperature of 1,10-decanediol, resulting in the heat not being absorbed, and at this time, the heat will be preferentially transferred to the regions with lower temperatures, i.e., the heat will be transferred from the P_3 region to the P_1 region, and from the P_4 region to the P_2 region. This can also be seen in the infrared thermography image in Fig. 5(f), where the high-temperature region diffuses to the low-temperature region at the welding interface. This results in the P_1 and P_2 regions of module

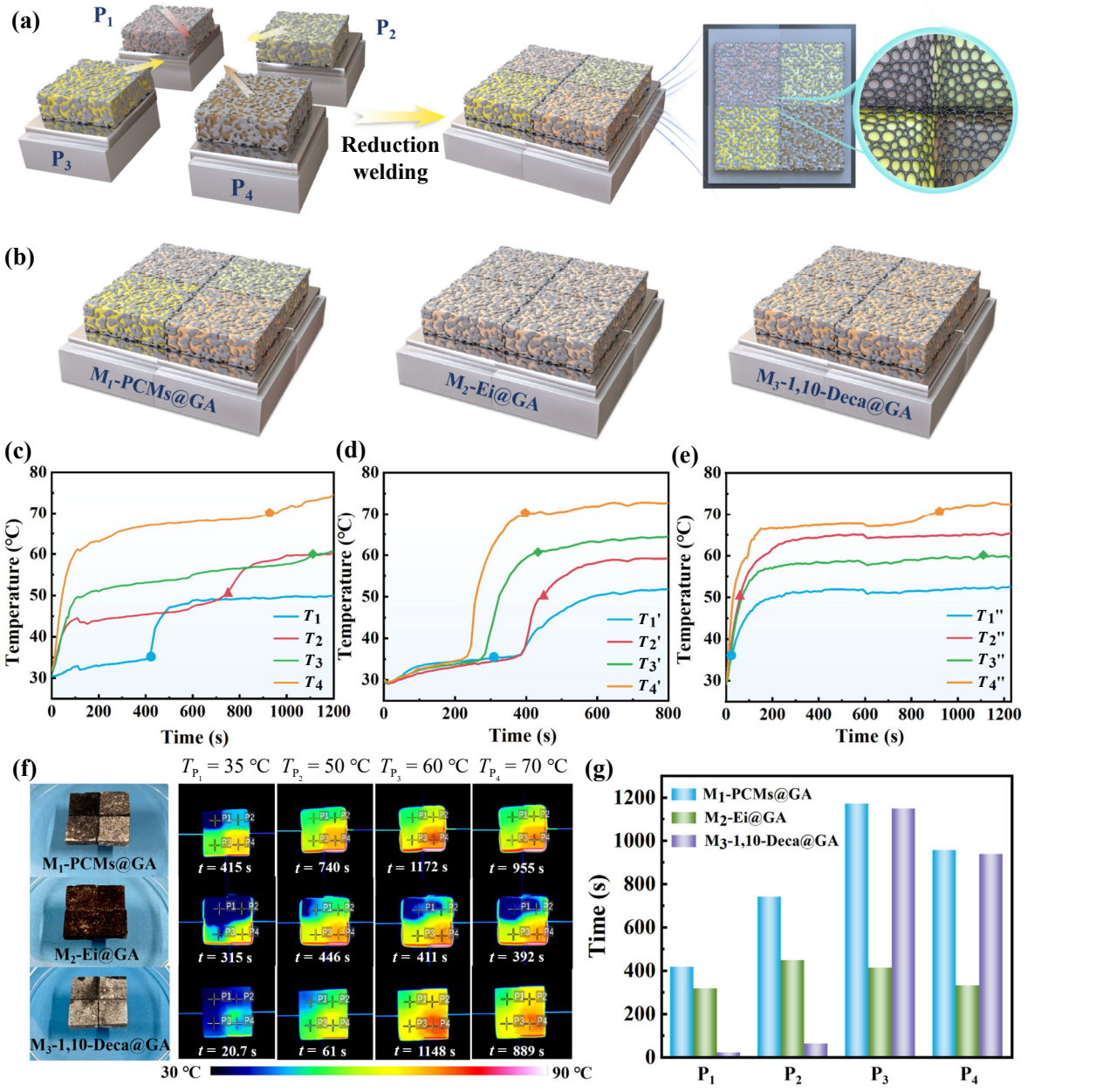

Figure 5 (a) Schematic diagram of the modular device assembly process. (b) Modeled diagrams of the modular spliced phase change composites M_1-PCMs@GA, M_2-Ei@GA, and M_3-1,10-Deca@GA. (c) Time–temperature profiles of the four parts of M_1-PCMs@GA, (d) time–temperature profiles of the four parts of M_2-Ei@GA, and (e) time–temperature profiles of the four parts of M_3-1,10-Deca@GA at the partitioned set temperature. (f) Physical drawings of M_1-PCMs@GA, M_2-Ei@GA, M_3-1,10-Deca@GA and infrared thermography pictures of each of the four regions when they reach a specific temperature control temperature. (g) Histograms of the time when each of the four regions of M_1-PCMs@GA, M_2-Ei@GA, and M_3-1,10-Deca@GA reached a specific temperature control temperature.

M_3-1,10-Deca@GA exceeding the upper temperature limit more quickly, while the P_3 and P_4 regions exhibit thermal management performance approximating the gradient splicing of module M_1-PCMs@GA.

The time to maintain the specific four zones below the ideal temperature is shown in Fig. 5(g), in which the data of the four zones of module M_1-PCMs@GA outperforms that of the comparison module, and the earliest time to exceed the ideal temperature zone is selected for comparison, and the temperature control time of M_1-PCMs@GA is 415.0 s, which compares with 315.0 s of M_2-Ei@GA and 21.0 s of M_3-1,10-Deca@GA were extended by 100.0 and 394.3 s, respectively. The experiment indicates that selecting the appropriate phase change molecule type for the regional heating characteristics of the electronic device can avoid the failure of the device due to rapid breakthrough of the temperature upper limit in the high temperature region, or the situation that the thermal management cannot be carried out in the low temperature region because the phase change temperature cannot be reached, and thus thermal management can be realized in a more efficient way. This provides new ideas for future customized heat dissipation components.

4 Summary

Overall, we prepared four different phase change composites by simple foaming method and vacuum impregnation with the

following excellent properties: the enthalpies of melting were as high as 209.5, 237.4, 245.5, and 263.1 J/g, with relative enthalpy efficiencies of more than 98.7%, and the enthalpy of the phase change was only lost by 0.4%–0.8% after 50 cycles, which is favorable for long-time thermal management. Owing to the formation of a three-dimensional continuous graphene aerogel skeleton, the thermal conductivity has been enhanced by over 20% compared to the original phase change material. The thermal stability is notably superior, with initial decomposition temperatures exceeding 110 °C, thus encompassing the majority of heat generation scenarios encountered in electronic devices. Additionally, the distinct phase change characteristics of the four phase change materials enable flexible selection for various heat generation scenarios. Furthermore, to address the non-uniformity of heat generation in practical applications, we developed a modular device M_1-PCMs@GA using the "reduction welding" method. In this device, the phase change composite materials in each of the four regions are chosen based on the regional temperature and the melting point of the phase change molecules. At the same time, the integrated design is easy to apply. In the actual thermal management test, the temperature control time of each region was extended compared with the homogeneous comparison devices M_2-Ei@GA and M_3-1,10-Deca@GA, and the overall effective temperature control time was extended by 100.0 and 394.3 s, respectively. Meanwhile, we observe that the temperature control duration is also influenced by the amount of phase change material. Therefore, in future modular assembly applications, both the type and quantity of the phase change material can be varied to achieve long-term temperature control at low temperatures and short-term temperature control at high temperatures. The modular temperature control devices developed in this study can handle more diverse and complex heat generation environments. The temperature-controlled gradient partitioning of heat generation can significantly enhance the efficiency of thermal management and broaden the application scenarios of phase change composites.

Electronic Supplementary Material: Supplementary material (structural characterizations, relevant thermophysical property data of PCMs and PCMs@GA, and appearance parameters of the modular devices) is available in the online version of this article at https://doi.org/10.26599/NR.2025.94907202.

Acknowledgements

This work was financially supported by the National Natural Science Foundation of China (Nos. 52327802, 52130303 and 52173078), the National Key R&D Program of China (No. 2022YFB3805702), Joint Funds of Ministry of Education (No. 8091B022225), and Tianjin University Science and Technology Leading Cultivation Program "Qiming Plan" (No. 2023XQM-0048).

Data availability

All data needed to support the conclusions in the paper are presented in the manuscript and the ESM. Additional data related to this paper may be requested from the corresponding author upon request.

Declaration of competing interest

The authors declare that they have no known competing financial interests or personal relationships that could have appeared to influence the work reported in this paper.

Author contribution statement

Y. L. C.: Conceptualization, data curation, formal analysis, writing – original draft, writing – review & editing. H. T. Y.: Formal analysis, investigation, writing – review & editing. Y. Y. F.: Conceptualization, funding acquisition, resources, writing – review & editing. W. F.: Funding acquisition, resources, supervision.

Use of AI statement

None.

References

[1] Khan, J.; Momin, S. A.; Mariatti, M. A review on advanced carbon-based thermal interface materials for electronic devices. *Carbon* **2020**, *168*, 65–112.

[2] Song, H. F.; Liu, J. M.; Liu, B. L.; Wu, J. Q.; Cheng, H. M.; Kang, F. Y. Two-dimensional materials for thermal management applications. *Joule* **2018**, *2*, 442–463.

[3] Song, N.; Cao, D. L.; Luo, X.; Wang, Q.; Ding, P.; Shi, L. Y. Highly thermally conductive polypropylene/graphene composites for thermal management. *Compos. Part A: Appl. Sci. Manuf.* **2020**, *135*, 105912.

[4] Wang, F. F.; Liu, Z. X.; Li, J. F.; Huang, J.; Fang, L.; Wang, X. F.; Dai, R. W.; Li, K. Y.; Zhang, R.; Yang, X. R. et al. Lateral heterostructure formed by highly thermally conductive fluorinated graphene for efficient device thermal management. *Adv. Sci.* **2024**, *11*, e2401586.

[5] Li, S. W.; Hou, D. M.; Cui, Y. S.; Jia, S.; Lan, G.; Sun, W. L.; Li, G. Y.; Li, X.; Feng, W. Highly ordered carbon aerogels: Synthesis, structures, properties and applications. *Carbon* **2024**, *218*, 118669.

[6] Y. X.; Ruan, K. P.; He, X. Y.; Tang, Y. S.; Guo, H.; Guo, Y. Q.; Qiu, H.; Gu, J. W. Highly thermally conductive aramid nanofiber composite films with synchronous visible/infrared camouflages and information encryption. *Angew. Chem., Int. Ed.* **2024**, *63*, e202401538.

[7] Wang, W.; Gong, Y. F.; Ren, H. W.; Wang, J.; Li, Q. M. High-temperature failure mechanism and lifetime assessment of silicone gel package insulation for high-power electronic devices based on pyrolysis kinetics. *IEEE Trans. Ind. Appl.* **2024**, *60*, 1298–1309.

[8] Zhang, Q. Y.; Feng, Z. F.; Zhang, J. X.; Guo, F. W.; Huang, S. Z.; Li, Z. Z. Design of a mini-channel heat sink for high-heat-flux electronic devices. *Appl. Therm. Eng.* **2022**, *216*, 119053.

[9] Wang, H. R.; Zhang, H.; Peng, L. Q.; Yu, H. T.; Qin, M. M.; Feng, Y. Y.; Feng, W. A versatile multilayer interwoven order-structured carbon-based building block for efficient heat dissipation. *Adv. Compos. Hybrid Mater.* **2024**, *7*, 101.

[10] Zhang, B.; Chen, X. M.; Pan, Z.; Liu, P.; Mao, M. M.; Song, K. X.; Mao, Z.; Sun, R.; Wang, D. W.; Zhang, S. J. Superior high-temperature energy density in molecular semiconductor/polymer all-organic composites. *Adv. Funct. Mater.* **2023**, *33*, 2210050.

[11] Yu, H. T.; Peng, L. Q.; Chen, C.; Qin, M. M.; Feng, W. Regulatable orthotropic 3D hybrid continuous carbon networks for efficient Bi-directional thermal conduction. *Nano-Micro Lett.* **2024**, *16*, 198.

[12] Gholipour, B. The promise of phase-change materials. *Science* **2019**, *366*, 186–187.

[13] Shi, J. M.; Qin, M. L.; Aftab, W.; Zou, R. Q. Flexible phase change materials for thermal energy storage. *Energy Storage Mater.* **2021**, *41*, 321–342.

[14] Wang, P.; Diao, X. M.; Chen, X. Intelligent phase change materials for long-duration thermal energy storage. *Matter* **2024**, *7*, 2716–2718.
[15] Tao, J. L.; Luan, J. D.; Liu, Y.; Qu, D. Y.; Yan, Z.; Ke, X. Technology development and application prospects of organic-based phase change materials: An overview. *Renewable Sustainable Energy Rev* **2022**, *159*, 112175.
[16] Xie, Y. F.; Yang, Y. P.; Liu, Y.; Wang, S. T.; Guo, X. X.; Wang, H.; Cao, D. P. Paraffin/polyethylene/graphite composite phase change materials with enhanced thermal conductivity and leakage-proof. *Adv. Compos. Hybrid Mater.* **2021**, *4*, 543–551.
[17] Yang, J.; Zhou, Y. C.; Yang, L. Y.; Feng, C. P.; Bai, L.; Yang, M. B.; Yang, W. Exploring next-generation functional organic phase change composites. *Adv. Funct. Mater.* **2022**, *32*, 2200792.
[18] Li, X. L.; Sheng, X. X.; Guo, Y. Q.; Lu, X.; Wu, H.; Chen, Y.; Zhang, L.; Gu, J. W. Multifunctional HDPE/CNTs/PW composite phase change materials with excellent thermal and electrical conductivities. *J. Mater. Sci. Technol.* **2021**, *86*, 171–179.
[19] Fu, L. L.; Wang, Q. H.; Ye, R. D.; Fang, X. M.; Zhang, Z. G. A calcium chloride hexahydrate/expanded perlite composite with good heat storage and insulation properties for building energy conservation. *Renewable Energy* **2017**, *114*, 733–743.
[20] Liang, K. C.; Zhang, H.; Wang, Q. W.; Cheng, Z. L. PVA-assisted graphene aerogels composite phase change materials with anisotropic porous structure for thermal management. *Carbon* **2024**, *230*, 119639.
[21] Ling, Z. Y.; Zhang, Z. G.; Shi, G. Q.; Fang, X. M.; Wang, L.; Gao, X. N.; Fang, Y. T.; Xu, T.; Wang, S. F.; Liu, X. H. Review on thermal management systems using phase change materials for electronic components, Li-ion batteries and photovoltaic modules. *Renewable Sustainable Energy Rev.* **2014**, *31*, 427–438.
[22] Liu, H.; Tian, X. X.; Ouyang, M. Z.; Wang, X.; Wu, D. Z.; Wang, X. D. Microencapsulating n-docosane phase change material into $CaCO_3/Fe_3O_4$ composites for high-efficient utilization of solar photothermal energy. *Renewable Energy* **2021**, *179*, 47–64.
[23] Luo, Z.; Yang, D. Z.; Liu, J.; Zhao, H. Y.; Zhao, T. Y.; Li, B. X.; Yang, W. G.; Yu, Z. Z. Nature-inspired solar-thermal gradient reduced graphene oxide aerogel-based bilayer phase change composites for self-adaptive personal thermal management. *Adv. Funct. Mater.* **2023**, *33*, 2212032.
[24] He, Q. X.; Qin, M. M.; Zhang, H.; Yue, J. W.; Peng, L. Q.; Liu, G. J.; Feng, Y. Y.; Feng, W. Patterned liquid metal embedded in brush-shaped polymers for dynamic thermal management. *Mater. Horiz.* **2024**, *11*, 531–544.
[25] Yun, J.; Yoo, Y. J.; Kim, H. R.; Song, Y. M. Recent progress in thermal management for flexible/wearable devices. *Soft Sci.* **2023**, *3*, 12.
[26] Liang, C. B.; Huo, Q. Q.; Qi, J. M.; Zhang, Y. L.; Liu, C. L.; Liu, Y. Q.; Gu, J. W. Robust solid-solid phase change coating encapsulated glass fiber fabric with electromagnetic interference shielding for thermal management and message encryption. *Adv. Funct. Mater.* **2024**, *34*, 2409146.
[27] Chen, Y. H.; Meng, Y.; Zhang, J. Y.; Xie, Y. H.; Guo, H.; He, M. K.; Shi, X. T.; Mei, Y.; Sheng, X. X.; Xie, D. L. Leakage proof, flame-retardant, and electromagnetic shield wood morphology genetic composite phase change materials for solar thermal energy harvesting. *Nano-Micro Lett.* **2024**, *16*, 196.
[28] Tu, J. Y.; Li, H. R.; Zhang, J. J.; Hu, D.; Cai, Z. Q.; Yin, X. Z.; Dong, L. J.; Huang, L. P.; Xiong, C. X.; Jiang, M. Latent heat and thermal conductivity enhancements in polyethylene glycol/polyethylene glycol-grafted graphene oxide composites. *Adv. Compos. Hybrid Mater.* **2019**, *2*, 471–480.
[29] Guo, H.; Hu, B. Y.; Shan, H. T.; Li, Z.; Qi, W. Y.; Li, B. A. Magnetically assembled flexible phase change composites with vertically aligned structures for thermal management and electromagnetic interference shielding. *Chem. Eng. J.* **2024**, *495*, 153361.
[30] Hu, Y.; Zhang, M. Y.; Quan, B. Q.; Li, X. L.; Hu, X. P.; Wu, H.; Huang, X. R.; Lu, X.; Qu, J. P. Polyethylene glycol infiltrated biomass-derived porous carbon phase change composites for efficient thermal energy storage. *Adv. Compos. Hybrid Mater.* **2024**, *7*, 68.
[31] Li, M. X.; Wang, X. J.; Shen, J. H.; Zhao, D.; Lian, J. Phase change-related thermal property characterization and enhancement in carbon-based organic phase change composites. *Appl. Phys. Rev.* **2024**, *11*, 021322.
[32] Min, P.; Liu, J.; Li, X. F.; An, F.; Liu, P. F.; Shen, Y. X.; Koratkar, N.; Yu, Z. Z. Thermally conductive phase change composites featuring anisotropic graphene aerogels for real-time and fast-charging solar-thermal energy conversion. *Adv. Funct. Mater.* **2018**, *28*, 1805365.
[33] Wang, C. H.; Lin, T.; Li, N.; Zheng, H. P. Heat transfer enhancement of phase change composite material: Copper foam/paraffin. *Renewable Energy* **2016**, *96*, 960–965.
[34] Wang, J. X.; Mao, Y. F.; Miljkovic, N. Nano-enhanced graphite/phase change material/graphene composite for sustainable and efficient passive thermal management. *Adv. Sci.* **2024**, *11*, 2402190.
[35] He, M. K.; Zhong, X.; Lu, X. H.; Hu, J. W.; Ruan, K. P.; Guo, H.; Zhang, Y. L.; Guo, Y. Q.; Gu, J. W. Excellent low-frequency microwave absorption and high thermal conductivity in polydimethylsiloxane composites endowed by hydrangea-like CoNi@BN heterostructure fillers. *Adv. Mater.* **2024**, *36*, 2410186.
[36] Cao, Y.; Weng, M. M.; Mahmoud, M. H. H.; Elnaggar, A. Y.; Zhang, L.; El Azab, I. H.; Chen, Y.; Huang, M. N.; Huang, J. T.; Sheng, X. X. Flame-retardant and leakage-proof phase change composites based on MXene/polyimide aerogels toward solar thermal energy harvesting. *Adv. Compos. Hybrid Mater.* **2022**, *5*, 1253–1267.
[37] Wu, S.; Li, T. X.; Wu, M. Q.; Xu, J. X.; Hu, Y. H.; Chao, J. W.; Yan, T. S.; Wang, R. Z. Highly thermally conductive and flexible phase change composites enabled by polymer/graphite nanoplatelet-based dual networks for efficient thermal management. *J. Mater. Chem. A* **2020**, *8*, 20011–20020.
[38] Wang, C. X.; Liu, Q.; Song, H. J.; Jiang, Q. L. Vacuum filtration method towards flexible thermoelectric films. *Soft Sci.* **2023**, *3*, 34.
[39] Yue, Y.; Li, X. Y.; Zhao, Z. F.; Wang, H.; Guo, X. G. Stretchable flexible sensors for smart tires based on laser-induced graphene technology. *Soft Sci.* **2023**, *3*, 13.
[40] Wu, Y. G.; Dong, S.; Li, X. J.; Wen, L. G.; Shen, H. W.; Li, M. J.; Liu, X.; Zhang, Y.; Zeng, G. L.; Zheng, J. Y. et al. A stretchable all-nanofiber iontronic pressure sensor. *Soft Sci.* **2023**, *3*, 33.
[41] Yu, H. Y.; Gai, M. X.; Liu, L.; Chen, F. R.; Bian, J.; Huang, Y. A. Laser-induced direct graphene patterning: From formation mechanism to flexible applications. *Soft Sci.* **2023**, *3*, 4.
[42] Sultanov, F.; Tatykayev, B.; Bakenov, Z.; Mentbayeva, A. The role of graphene aerogels in rechargeable batteries. *Adv. Colloid Interface Sci.* **2024**, *331*, 103249.
[43] Wu, Y.; An, C.; Guo, Y. R.; Zong, Y. Y.; Jiang, N. S.; Zheng, Q. B.; Yu, Z. Z. Highly aligned graphene aerogels for multifunctional composites. *Nano-Micro Lett.* **2024**, *16*, 118.
[44] Honda, S. A preliminary analysis of convection in a mantle with a heterogeneous distribution of heat-producing elements. *Phys. Earth Planet. Inter.* **1984**, *34*, 68–76.
[45] Ping, P.; Zhang, Y.; Kong, D. P.; Du, J. Investigation on battery thermal management system combining phase changed material and liquid cooling considering non-uniform heat generation of battery. *J. Energy Storage* **2021**, *36*, 102448.
[46] Huang, Y. Q.; Wei, C. F.; Fang, Y. D. Numerical investigation on optimal design of battery cooling plate for uneven heat generation conditions in electric vehicles. *Appl. Therm. Eng.* **2022**, *211*, 118476.
[47] Wu, B.; Yufit, V.; Marinescu, M.; Offer, G. J.; Martinez-Botas, R. F.; Brandon, N. P. Coupled thermal-electrochemical modelling of uneven heat generation in lithium-ion battery packs. *J. Power Sources* **2013**, *243*, 544–554.
[48] Yang, P.; Wu, B.; Tong, X.; Zeng, M.; Wang, Q. W.; Cheng, Z. L.

Insight into heat transfer process of graphene aerogel composite phase change material. *Energy* **2023**, *279*, 128051.
[49] Yang, H. S.; Li, Z. L.; Sun, G. Q.; Jin, X. T.; Lu, B.; Zhang, P. P.; Lin, T. Y.; Qu, L. T. Superplastic air-dryable graphene hydrogels for wet-press assembly of ultrastrong superelastic aerogels with infinite macroscale. *Adv. Funct. Mater.* **2019**, *29*, 1901917.
[50] Zhang, X. F.; Zhang, T. P.; Wang, Z.; Ren, Z. J.; Yan, S. K.; Duan, Y. X.; Zhang, J. M. Ultralight, superelastic, and fatigue-resistant graphene aerogel templated by graphene oxide liquid crystal stabilized air bubbles. *ACS Appl. Mater. Interfaces* **2019**, *11*, 1303–1310.
[51] Fang, Z. H.; Luo, Y. F.; Wu, H. C.; Yan, L. J.; Zhao, F.; Li, Q. Q.; Fan, S. S.; Wang, J. P. Mesoporous carbon nanotube aerogel-sulfur cathodes: A strategy to achieve ultrahigh areal capacity for lithium-sulfur batteries via capillary action. *Carbon* **2020**, *166*, 183–192.
[52] Liyanage, C. D.; Kumar, H.; Perera, I.; Abeykoon, P. G.; Chen, F. Y.; Joya, J. S.; Suib, S. L.; Adamson, D. H. Synthesis of graphene oxide: Effect of sonication during oxidation. *Carbon* **2024**, *223*, 119047.
[53] Ye, Y. S.; Huang, W. X.; Xu, R.; Xiao, X.; Zhang, W. B.; Chen, H.; Wan, J. Y.; Liu, F.; Lee, H. K.; Xu, J. W. et al. Cold-starting all-solid-state batteries from room temperature by thermally modulated current collector in sub-minute. *Adv. Mater.* **2022**, *34*, 2202848.
[54] Zhu, P. Y.; Shen, M.; Xiao, S. H.; Zhang, D. Experimental study on the reducibility of graphene oxide by hydrazine hydrate. *Phys. B: Condens. Matter* **2011**, *406*, 498–502.
[55] Liu, H. L.; Yang, C.; Wei, B.; Jin, L.; Alatas, A.; Said, A.; Tongay, S.; Yang, F.; Javey, A.; Hong, J. W. et al. Anomalously suppressed thermal conduction by electron-phonon coupling in charge-density-wave tantalum disulfide. *Adv. Sci.* **2020**, *7*, 1902071.
[56] Nakashima, A.; Sagawa, Y.; Kimura, M. Temperature sensor using thin-film transistor. *IEEE Sens. J.* **2011**, *11*, 995–998.